Article

Molecular Cell

Loss of Dynamic RNA Interaction and Aberrant Phase Separation Induced by Two Distinct Types of ALS/FTD-Linked FUS Mutations

Graphical Abstract

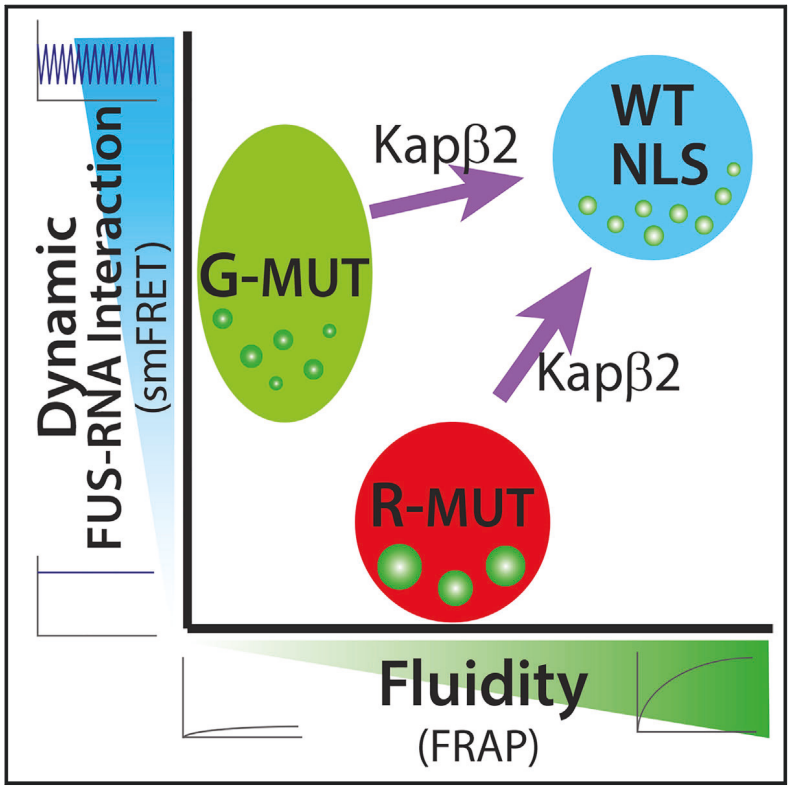

Authors

Amirhossein Ghanbari Niaki, Jaya Sarkar, Xinyi Cai, ..., Charlotte M. Fare, James Shorter, Sua Myong

Correspondence

smyong@jhu.edu

In Brief

FUS aggregation is pathogenic hallmark of incurable neurodegenerative diseases, including ALS and FTD. Niaki et al. demonstrate that two classes of ALS/FTD-linked mutations display distinct molecular phenotypes. Arginine mutations lead to defective RNA binding, whereas glycine mutations induce quick loss of fluidity, underpinning potentially disparate pathogenic pathways of disease-linked FUS mutants.

Highlights

- FUS multimer interacts dynamically with RNA, resulting in liquid-like condensates
- ALS/FTD-linked FUS mutations in arginine lead to defective RNA binding
- ALS/FTD-linked FUS mutations in glycine induce quick loss of condensate fluidity
- Karyopherin- β2 reverses mutant defects and recovers wild-type FUS properties

Niaki et al., 2020, Molecular Cell *77*, 82–94
January 2, 2020
https://doi.org/10.1016/j.molcel.2019.09.022

CellPress

CellPress

Molecular Cell
Article

Loss of Dynamic RNA Interaction and Aberrant Phase Separation Induced by Two Distinct Types of ALS/FTD-Linked FUS Mutations

Amirhossein Ghanbari Niaki,[1,9] Jaya Sarkar,[1,9] Xinyi Cai,[1] Kevin Rhine,[2] Velinda Vidaurre,[2] Brian Guy,[2] Miranda Hurst,[1] Jong Chan Lee,[3] Hye Ran Koh,[1,4] Lin Guo,[5,6] Charlotte M. Fare,[6,7] James Shorter,[6,7] and Sua Myong[1,8,10,*]

[1]T.C. Jenkins Department of Biophysics, Johns Hopkins University, 3400 N. Charles St., Baltimore, MD 21218, USA
[2]Cellular Molecular Developmental Biology and Biophysics, Johns Hopkins University, 3400 N. Charles St., Baltimore, MD 21218, USA
[3]Department of Biophysics and Biophysical Chemistry and Department of Biomedical Engineering, Johns Hopkins University, Baltimore, MD 21205, USA
[4]Department of Chemistry, Chung-Ang University, Seoul 054974, Korea
[5]Department of Biochemistry and Molecular Biology, Jefferson University, Philadelphia, PA 19107, USA
[6]Department of Biochemistry and Biophysics, Perelman School of Medicine, University of Pennsylvania, Philadelphia, PA 19104, USA
[7]Biochemistry and Molecular Biophysics Graduate Group, Perelman School of Medicine, University of Pennsylvania, Philadelphia, PA 19104, USA
[8]Department of Physics, Center for the Physics of Living Cells and Institute for Genomic Biology, University of Illinois at Urbana-Champaign, Urbana, IL 61801, USA
[9]These authors contributed equally
[10]Lead Contact
*Correspondence: smyong@jhu.edu
https://doi.org/10.1016/j.molcel.2019.09.022

SUMMARY

FUS is a nuclear RNA-binding protein, and its cytoplasmic aggregation is a pathogenic signature of amyotrophic lateral sclerosis (ALS) and frontotemporal dementia (FTD). It remains unknown how the FUS-RNA interactions contribute to phase separation and whether its phase behavior is affected by ALS-linked mutations. Here we demonstrate that wild-type FUS binds single-stranded RNA stoichiometrically in a length-dependent manner and that multimers induce highly dynamic interactions with RNA, giving rise to small and fluid condensates. In contrast, mutations in arginine display a severely altered conformation, static binding to RNA, and formation of large condensates, signifying the role of arginine in driving proper RNA interaction. Glycine mutations undergo rapid loss of fluidity, emphasizing the role of glycine in promoting fluidity. Strikingly, the nuclear import receptor Karyopherin-β2 reverses the mutant defects and recovers the wild-type FUS behavior. We reveal two distinct mechanisms underpinning potentially disparate pathogenic pathways of ALS-linked FUS mutants.

INTRODUCTION

Fused in sarcoma (FUS) is an RNA-binding protein (RBP) involved in an array of RNA metabolic processes and the formation of ribonucleoprotein (RNP) bodies such as stress granules (SGs) (Lagier-Tourenne et al., 2010; Protter and Parker, 2016). RNP bodies are proposed to form by liquid-liquid phase separation (LLPS), driven by transient multivalent interactions between RNA and RBPs containing intrinsically disordered regions (IDRs) and RNA recognition motifs (RRMs) (Guo and Shorter, 2015; Hyman et al., 2014; Weber and Brangwynne, 2012). Indeed, FUS features an extensive prion-like domain (PRLD) at its N terminus, an RRM in the middle, and RGG domains at the C terminus (Figure S1A). Mutations in FUS and other SG RBPs (such as TDP-43 and hnRNPA1) are causative agents of neurodegenerative diseases such as amyotrophic lateral sclerosis (ALS) and frontal temporal dementia (FTD) (Aulas and Vande Velde, 2015; Bosco et al., 2010; Kang et al., 2018; Kapeli et al., 2017; Li et al., 2013; Ling et al., 2013; Mackenzie and Neumann, 2017; Nolan et al., 2016; Nomura et al., 2014; Stoica et al., 2016; Svetoni et al., 2016). ALS/FTD mutants of FUS incorporate into normal fluid SGs and induce conversion to irreversible pathological aggregates in the course of disease progression (Vance et al., 2009).

Numerous ALS/FTD-associated mutations in FUS are clustered in the IDR, which is necessary and sufficient for driving LLPS (Burke et al., 2015; Lin et al., 2015; Molliex et al., 2015; Patel et al., 2015). Previous studies focused primarily on protein-only systems and neglected the role of RNA and RNA-protein interactions in phase separation. However, the emerging view acknowledges a cooperative effect of RNA-RNA (Jain and Vale, 2017; Van Treeck et al., 2018), RNA-protein, and protein-protein interactions in RNP granule assembly and disease progression. RNA can seed FUS and hnRNPA1 droplets by increasing multivalent interactions (Burke et al., 2015; Molliex et al., 2015; Schwartz et al., 2013). We and others have reported that RNA differentially affects the *in vitro* viscoelastic properties of Whi3 and LAF-1 droplets (Elbaum-Garfinkle et al., 2015;

Zhang et al., 2015). Our earlier work also demonstrated that RNA structure is critical in establishing granule identity and the RNA-protein interactions to maintain granule identity in the Whi3 system (Langdon et al., 2018). In mammalian cells, RNA buffers phase separation of FUS and RBPs; the high RNA-to-protein ratio in the nucleus keeps RBPs soluble, whereas the low ratio in the cytoplasm promotes condensation (Maharana et al., 2018a). In fact, the RNA-binding ability of ALS mutant FUS is what allows the protein to localize to SGs, where it exhibits a neurodegenerative phenotype (Daigle et al., 2013), reinforcing the role of RNA in granule formation and disease onset. Nevertheless, a fundamental molecular-level understanding of how the initial interaction of RNA and IDR proteins affects LLPS and drives the disease phenotype is lacking. In this study, we address this gap by directly probing RNA interactions with FUS, one of the major proteins implicated in ALS/FTD.

We sought to address the question of "when does the mutation become aberrant?" by studying RNA-protein interactions with wild-type (WT) FUS as well as several classes of ALS-linked mutations: five arginine (R) mutations (R216C, R244C, R514G, R521C, and R521G), five glycine (G) mutations (G156E, G187S, G225V, G230C, and G399V), two nuclear localization sequence (NLS) mutations (R495X and P525L), and two non-ALS control mutations (R244K and R244A). Our results reveal that FUS-WT binds RNA stoichiometrically in an RNA length-dependent manner. Although a monomer binds RNA in two steps to establish a stable interaction, multimers (two and three units) of FUS-WT interact dynamically with RNA. Strikingly, R244C, a single ALS-associated point mutant, exhibits altered binding of RNA from the initial moment of contact, leading to highly static interactions with RNA and build-up of aggregation. Such altered RNA binding is shared among all R mutants, consistently leading to formation of larger condensates with diminished fluidity, strongly suggesting that arginine is important for FUS to engage properly with RNA. In contrast, G mutants display RNA binding and dynamics comparable with FUS-WT but phase-separate into small gel- or solid-like condensates, reflecting the major role of glycine in contributing to the condensate fluidity. Unlike R and G mutants, the NLS mutants resemble FUS-WT in all aspects of RNA binding, confirming that the NLS is a functionally separate domain that does not affect RNA binding or FUS-FUS interaction in a major way. The marked difference exhibited by R and G mutants reveals unique molecular aberrations that may lead to different pathogeneses. Notably, Karyopherin-β2 (Kapβ2) not only dissolves the R and G mutant condensates but also reverses the defective RNA binding, recovering the FUS-WT interaction with RNA. Taken together, we posit a plausible molecular connection between FUS-RNA interaction and phase separation in WT versus ALS mutant FUS.

RESULTS

FUS-RNA Interaction Probed by smFRET Reveals Two Modes of Interaction

We used single-molecule Förster resonance energy transfer (smFRET) to probe the interaction between FUS-WT and RNA. We prepared human full-length FUS by recombinant expression with an MBP tag at the N terminus for solubility and hexa-histidine for purification by Ni-NTA affinity column (Figures S1B and S1C; STAR Methods). Because FUS interacts with single-stranded RNA (ssRNA) (Wang et al., 2015), we prepared an RNA substrate with FRET pair dyes (Cy3 and Cy5) separated by 50 nt of poly-uracil (pdU50 for partial duplex U50) (Figure 1A; STAR Methods; Kim and Myong, 2016). We chose a simple unstructured homopolymer of ssRNA because FUS is a promiscuous RNA binder known to bind RNAs with or without cognate FUS-binding motifs with similar affinity (Lagier-Tourenne et al., 2012; Wang et al., 2015). The resulting FRET value of pdU50 on its own is approximately 0.2, shown as a single FRET peak generated by collecting FRET values from over 2,000 immobilized RNA molecules. Addition of FUS even at low concentrations (5 nM) immediately shifts the low FRET (0.2) to a single high FRET peak (0.8), indicating that the two dyes are being brought into close proximity (Figure 1B). Single-molecule traces display a stable high FRET signal, suggesting that FUS induces tight compaction of long ssRNA.

As FUS concentration increases (50–500 nM), the high FRET population diminishes, whereas a broad mid-FRET peak (~0.5) emerges (Figure 1B, right panel), concomitant with fluctuation of the smFRET traces (Figure 1B, left panel). The FRET fluctuation is a dominant pattern seen in more than 90% of all traces obtained at 200–500 nM FUS concentration. If the FRET fluctuation were to arise from successive binding and unbinding of FUS molecules to RNA or existing FUS-RNA complexes, then we would expect the rate of fluctuation to increase as a function of protein concentration (Figure S1A). However, the frequency of the FRET fluctuations observed at different FUS concentrations remained unchanged (Figure 1C), strongly suggesting that the FRET fluctuations arise from bound FUS species interacting dynamically with the ssRNA. Removal of the excess protein returned the RNA to the stable high FRET state observed at low FUS concentrations, suggesting that the dynamic state is a weakly engaged, transient state of the FUS-RNA complex.

To test potential stoichiometric changes of the FUS-RNA complex, we used an electrophoretic mobility shift assay (EMSA) with the same RNA construct used in the single-molecule assay and varying concentrations of FUS (Figures 1D and 1E). The pattern of mobility shift indicates that FUS binding to RNA induces a single-shifted band (complex 1 [C1]) at low protein concentrations (2–10 nM) and a second super-shifted band (complex 2 [C2]) at higher protein concentrations (50–500 nM) (Figures 1D and 1E). Interestingly, there is a linear correlation between the fraction of C2 in EMSA and the percentage of single-molecule traces that exhibit FRET fluctuations (Figure 1F), suggesting that dynamic FUS-RNA interactions arise from the species represented by C2. Next, we further tested the stoichiometry by preparing FUS tagged with a C-terminal GFP tag (Figures S1B and S1C). We immobilized the same RNA construct, pdU50, labeled with Cy5 (for localization) and applied various FUS-GFP concentrations (Figure 1G). Because of the high fluorescence background, we could not take measurements above a concentration of 10 nM FUS-GFP. At 2–5 nM, FUS-GFP displayed mostly single-step photobleaching, (Figure 1H and 1J), which revealed predominantly monomer FUS-GFP bound to RNA after subtracting GFP-induced dimers (~30%) (Figure S1E; STAR Methods). At 10–50 nM FUS-GFP, two-step photobleaching emerged in a

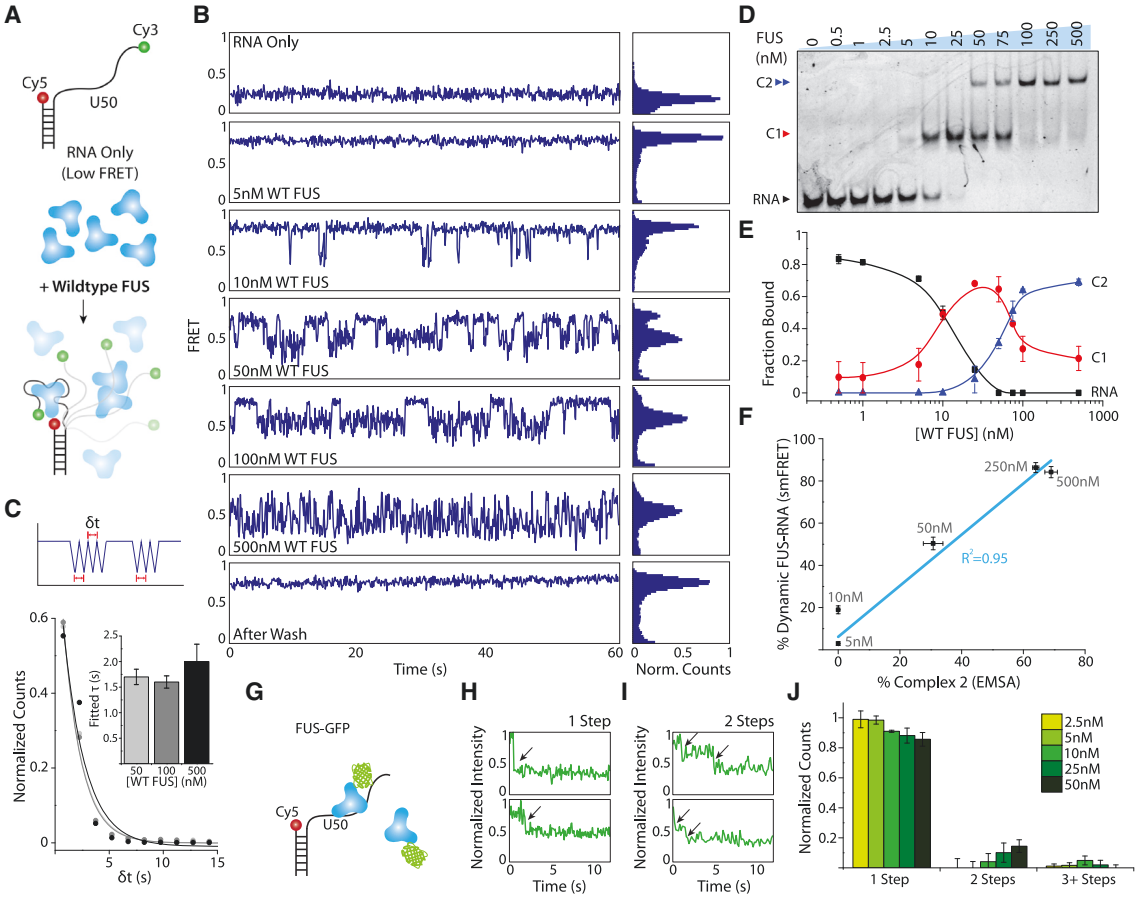

Figure 1. WT FUS Interacts with RNA in Two Modes

(A) Schematic of the smFRET experiment in which Cy3 and Cy5 attached to either end of U50 RNA report on the conformational change induced by FUS binding.

(B) smFRET representative traces and histograms for increasing FUS concentrations (0–500 nM) and after buffer wash of free protein in solution.

(C) Dwell time analysis of the dynamic FRET fluctuations at 50, 100, and 500 nM FUS fitted with a single-component exponential decay, with the bar graph representing the mean and SD of the fitted decay time.

(D) EMSA gel using pdU50 RNA (2 nM) at increasing FUS concentrations (0–500 nM). The arrows indicate bands representing RNA alone, complex 1 (C1), and complex 2 (C2).

(E) Quantification of EMSA band intensity.

(F) Correlation plot (R^2 = 0.95) between the fraction of C2 observed in the EMSA and the fraction of dynamic FRET traces at different FUS concentrations with SD.

(G) GFP-FUS experimental scheme used to count photobleaching steps to determine the stoichiometry of RNA:FUS at varying FUS conditions.

(H and I) Representative single-molecule trace of one-step (H) and two-step (I) photobleaching. Arrows indicate individual photobleaching steps.

(J) GFP photobleaching counts for different FUS concentrations after subtracting the inherent dimerization because of GFP alone (Figure S1; STAR Methods).

small population of molecules (~15% at 50 nM), likely indicating a stoichiometric shift from the C1 to the C2 state (Figures 1I and 1J). The small fraction of two steps is likely responsible for the short burst of dynamic FRET fluctuations observed at 10 nM (Figure 1B). In addition, we confirmed that FUS-GFP displays the same interaction with RNA as FUS-WT (Figure S1D). Taken together, C1 represents a FUS monomer interacting stably with ssRNA, yielding a steady high FRET signal, whereas C2 is likely two units of FUS engaging weakly with RNA, establishing highly dynamic interactions.

RNA Length Controls FUS Occupancy

We next asked whether RNA length plays a role in controlling the valency for FUS binding. To test this, we prepared a series of FRET-labeled RNA with varying lengths of poly-uracil (Figure 2A). All of the Cy3-labeled poly-uracil (polyU) strands (U10–U70; Figure 2A, left panel) were annealed to the same Cy5- and biotin-labeled 18-mer RNA strand with a complementary sequence, resulting in pdU10–pdU70 (Figure 2A, right panel). The native gel displays a clear separation of mobility shift of both the single-stranded and the partially duplexed RNA forms (Figure 2A). These constructs were individually tested in the smFRET assay with FUS-WT. Upon addition of FUS-WT (500 nM), the FRET peaks shifted from lower (Figure 2B, light gray histograms) to higher values in all cases, confirming that FUS binds to all lengths of RNA (Figure 2B, dark blue histograms). FUS binding to pdU10–pdU30 produced a sharp high FRET peak with corresponding stable high FRET traces (Figure 2B). For pdU40, the static high FRET signal is interspersed by bursts of FRET fluctuations. By contrast, FUS binding to pdU50 and pdU70 yielded

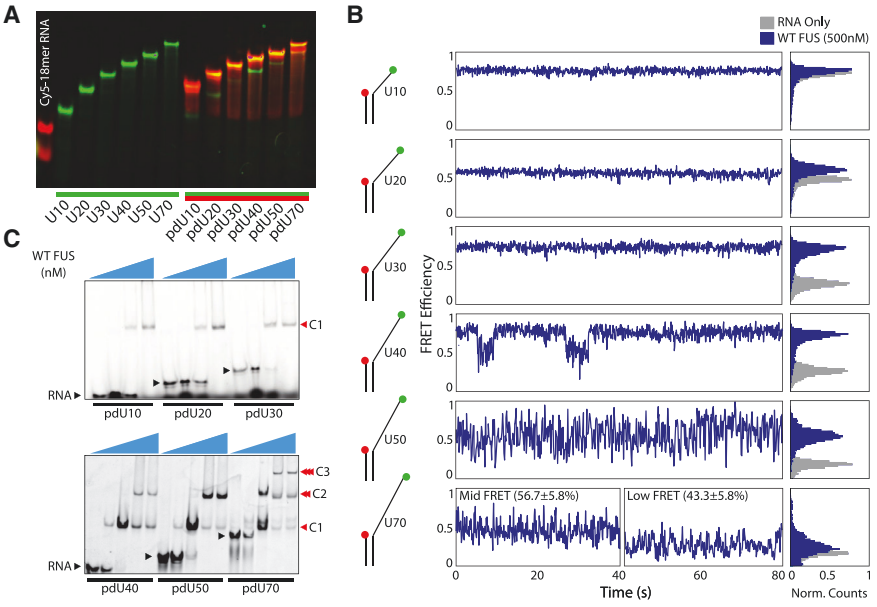

Figure 2. RNA Length Controls FUS Multivalency

(A) Native gel showing Cy3-labeled polyU (U10–U70) and partially duplexed pdU10–pdU70.

(B) Representative FRET traces at varying RNA lengths, taken with 500 nM FUS and FRET histograms for varying RNA lengths in the absence (light gray) and presence (dark blue) of 500 nM FUS (right).

(C) EMSA gels for pdU10–pdU70 at increasing concentrations of FUS (0–500 nM). Demarcations for unbound RNA (black arrow), C1, C2, and C3 are shown.

significantly broader FRET peaks that arise from sustained FRET fluctuations displayed in single-molecule FRET traces (Figure 2B). Interestingly, pdU70 rendered two classes of FRET fluctuations: one in a mid-FRET range (0.4–0.7) and the other with low FRET (0.2–0.5) amplitudes, which we relate to C2 and C3 stoichiometric states, as demonstrated below (Figure S2).

Analysis by EMSA gels revealed that FUS (0, 5, 50, or 500 nM) binding to pdU10–pdU30 led to only C1 formation (Figure 2C). The FUS-pdU40 and pdU50 complex displayed clear C1 and C2, whereas FUS-pdU70 showed an additional supershifted band, complex 3 (C3) (Figure 2C). This strongly suggests that C1, C2, and C3 correspond to one, two, and three units of FUS bound to longer, 70-nt long RNA, which offers a higher valency because of its length. It is noteworthy that, despite the differences in molecular weight of RNA substrates (Figure 2A), all C1 and C2 FUS-RNA complexes show the same mobility shift in EMSA gels (Figure 2C), likely indicating extensive contact between RNA and protein, resulting in similar hydrodynamic radii for all RNP complexes containing varying lengths of RNA.

Together, the smFRET and EMSA results reveal that short lengths of RNA (up to U30) only allow a monomer of FUS to bind stably, producing a steady high FRET signal, whereas pdU40 and pdU50 accommodate two FUS molecules to bind, inducing a dynamic conformational change on the RNA. For pdU70, up to three FUS units can bind, giving rise to the mid- and low-range FRET fluctuations, likely representing the C2 and C3 states, respectively (Figures 2B and 2C; Figure S2). Here we establish that the length of RNA is important for regulating FUS valency and, thus, driving the multi-valent interactions.

R244C Displays Altered RNA Binding and Enhances Aggregation Propensity Because of Loss of Arginine

To test whether the ALS/FTD-linked mutations alter FUS:RNA interactions, we first investigated arginine mutations. Arginine is the most frequently mutated (approximately 30%) amino acid among ALS-linked FUS mutations, indicating that loss of arginine is a critical contribution to pathogenesis. Therefore, we chose five positions in which arginine is mutated (R216C, R244C, R514G, R521C, and R521G) and two non-ALS-linked substitutions (R244K and R244A) Here, we focus on one arginine mutation, R244C, and the two controls (R244K and R244A) (all mutants are shown in Figure 5). The R244C mutation is located within FUS's PRLD, adjacent to the RRM, and it is associated with severe neurological dysfunction in ALS patients (Kwiatkowski et al., 2009; Vance et al., 2009; Wang et al., 2013). We examined whether R244C's interaction with RNA is different from FUS-WT (Figure 3A). Unlike the WT, at 5 nM, R244C binding to RNA leads to two different FRET states in which smFRET traces show either static mid-FRET or high FRET states (Figure 3A). At higher concentrations (50–500 nM) of R244C, RNA molecules exhibit mainly static high FRET traces with infrequent excursions to mid-FRET states (Figure 3A). This is in stark contrast to the highly dynamic FUS-WT-RNA interaction in the same concentration range (Figure 1B; Figure S3). EMSA analysis reveals that R244C-RNA forms C1 but not C2 and aggregates at higher concentrations ($\geq$250 nM), visualized by thick smears near the loading wells (Figure 3B). The lack of C2 in the EMSA and negligible dynamics displayed in smFRET traces (Figure 3A) are consistent with the observation that C2 in the WT is generating the dynamic FUS-RNA interaction.

Next, we asked whether the altered RNA binding exhibited by R244C is due to loss of arginine or gain of cysteine by preparing non-ALS-linked variants, R244K and R244A. Lysine and alanine were chosen as conservative and non-conservative substitutions of arginine, respectively. If R244C's altered RNA interaction arises from loss of a positively charged arginine, then R244K should resemble FUS-WT, whereas R244A should mimic R244C. Indeed, we found that the smFRET result for R244K showed increasing levels of dynamic FRET fluctuations as a function of protein concentration (Figure 3C), highly similar to FUS-WT (Figure 1B). By contrast, R244A displays mainly static smFRET traces with infrequent dynamics (Figure 3D), similar to R244C (Figure 3A). The EMSA shows that R244K forms C2 starting from 25 nM concentration, concurrent with the emergence of smFRET dynamics, again similar to FUS-WT (Figure 1C). R244A, however, fails to form C2 even at high concentrations and

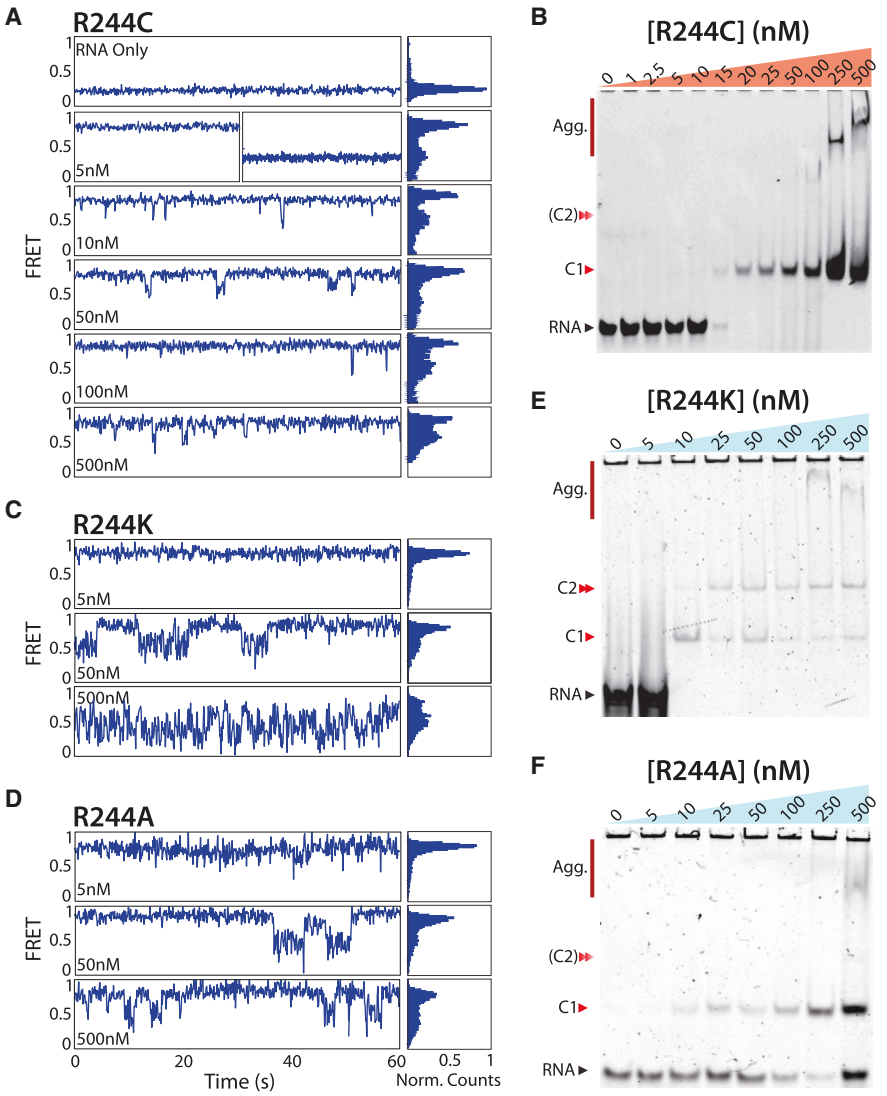

Figure 3. The R244C-RNA Interaction Is Altered Because of Loss of Arginine

(A, C, and D) Representative FRET traces and histograms for R244C (A), R244K (C), and R244A (D), taken at varying protein concentrations (5–500 nM).

(B, E, and F) EMSA gel using pdU50 at varying R244C (B), R244K (E), and R244A (F) concentrations; arrows denote the RNA band (black arrow), C1, the absence of complex 2 (C2), and aggregation.

aggregates (Figure 3F), resembling the R244C pattern (Figure 3B). We also observed a small degree of aggregation for R244K at high concentrations, which may be due to the arginine-to-lysine replacement, suggesting that arginine allows formation of C1 and C2 without aggregation. Taken together, we demonstrate that loss of the positively charged arginine in R244C and R244A is responsible for the altered interaction with RNA and that the R244C mutant may seed defective complex formation that drives the increased aggregation seen in disease. The substitution analysis strongly suggests that arginine is critical for properly engaging with RNA (C1) and that formation of C1 is necessary for formation of C2, which exhibits a dynamic interaction.

Defective RNA Binding of R244C Is Evident from the Beginning

The EMSA analysis shown in Figure 3B led us to hypothesize that the initial binding of a monomer (i.e., the formation of C1 complex) may be altered in R244C to block the proper engagement of the second FUS unit required for C2 formation. The EMSA pattern indicates that an altered C1 state persists as is or leads to large aggregated species at higher concentrations (Figure 3B). To test this hypothesis, we set up a real-time flow experiment in which smFRET videos were taken while adding WT or R244C FUS to RNA. These real-time videos allowed us to capture the initial moment when the protein contacts the RNA (Koh et al., 2014). First, we applied a low (2.5–5 nM) concentration of the WT at which only C1 should form. The addition of the WT (demarcated by a black vertical line) induced an immediate and well-defined two-step increase in FRET efficiency (Figure 4A, top), reflecting two well-separated steps involved in monomer binding. The heatmap generated by overlaying more than 100 traces confirms the dominant pattern of two-step binding of the WT monomer (Figure 4A, bottom). In contrast, R244C binding is significantly slower, exhibiting a poorly defined, low FRET state that does not transition to a high FRET state for more than 50 s (Figure 4B, top), resulting in a heatmap with a highly scattered pattern (Figure 4B, bottom).

To further investigate the binding mechanism of WT and R244C, we performed an alternative single-molecule method called protein-induced fluorescence enhancement (PIFE) (Hwang et al., 2011; Hwang and Myong, 2014). Briefly, a single dye attached to nucleic acid will become brighter upon contact with a protein, detected as an increase in fluorescence intensity. For our PIFE assay, we prepared two versions of the pdU50 construct, each with Cy3 dye at either end of the U50 so that FUS binding can be detected on either end independently (Qiu et al., 2013). Addition of the WT produced quick, clear, and uniform signal enhancement in both cases (~2×) (Figures 4C and 4E; Figures S4A and S4B), whereas R244C led to a substantially delayed, less distinct, and non-uniform signal increase (Figures 4D and 4E; Figures S4C and S4D), consistent with the irregular pattern observed in FRET measurement (Figure 4B). In addition, the clear time delay between the two PIFE experiments for the WT suggests that the protein makes contact with the tail end of pdU50 first before folding in closer to the single-stranded

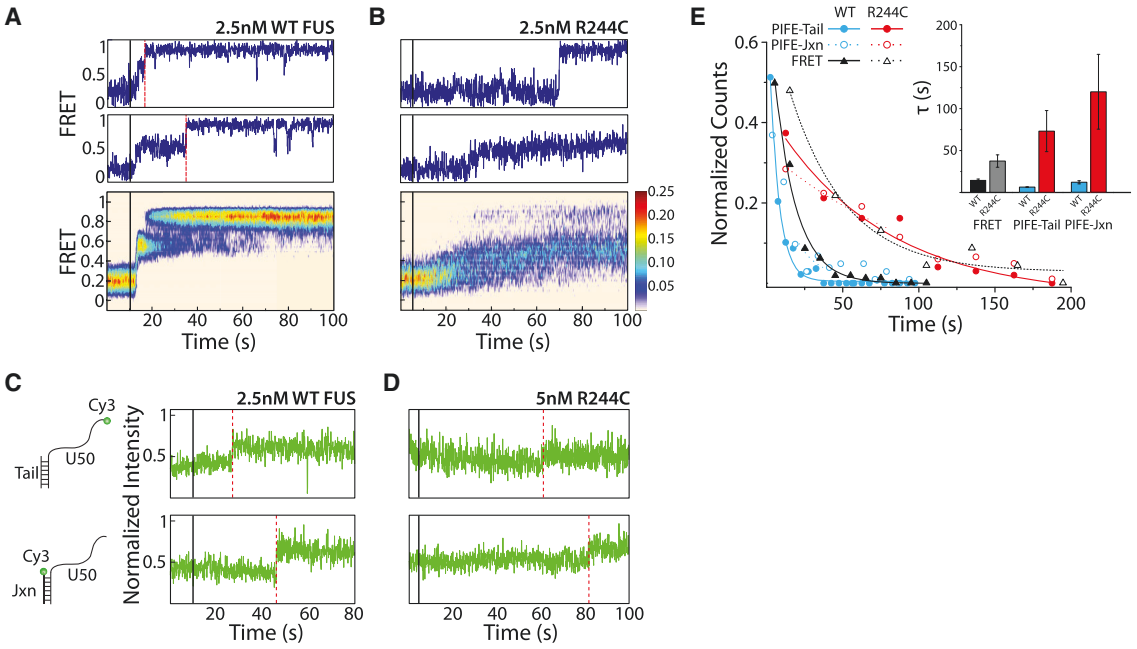

Figure 4. Initial R244C-RNA Binding Is Defective Compared with FUS-WT

(A and B) Representative real-time flow traces for 2.5 nM WT FUS (A) and R244C (B) added to FRET-labeled pdU50 RNA. The black lines mark the introduction of protein, and the red dashed line shows the transition to high FRET. The heatmaps are generated by overlaying more than 100 traces taken under each condition listed.

(C and D) PIFE flow experiment for the tail and junction (jxn) Cy3-labeled pdU50 at 2.5 nM WT FUS (C) and 5 nM R244C (D). The red dashed line indicates signal enhancement from protein binding.

(E) Quantification of the transition time taken by collecting the time required for FUS to bind RNA, observed by PIFE. The times were fitted with a single-component exponential decay with SD.

(ss)/double-stranded (ds) junction (Figures 4C and 4E), likely related to the two-step FRET increase observed above (Figure 4A). In summary, the initial binding of RNA by the WT occurs in a well-ordered two-step process, producing a stable C1, which leads to proper C2 formation. In contrast, R244C exhibits irregular binding to RNA so that it forms a defective C1 state that is incompatible with C2 formation, leading to aggregation at high concentrations (Figure 3B). The different pattern was also observed at higher protein concentrations (Figures S4E and S4F). The C1 band present in the EMSA gel across R244C concentrations signifies the persistent nature of the defective monomer-bound state. Together, our results provide strong evidence that proper formation of the C1 state is necessary for formation of a dynamic C2.

Arginine Mutants Display Diminished FUS-RNA Interaction Dynamics and No C2

We next prepared two NLS mutations, P525L and R495X, which are associated with an early-onset, highly aggressive form of ALS. The severity of these cases is due to defects in their nuclear import (Dormann et al., 2010) because of severely weakened interactions with the nuclear transporter Kapβ2. This results in cytoplasmic mislocalization and aggregation of FUS (Guo et al., 2018; Hofweber et al., 2018; Qamar et al., 2018; Yoshizawa et al., 2018). We asked whether these mutants' interactions with RNA are also affected. The smFRET assay carried out at a high (500 nM) protein concentration shows that both P525L and R495X establish highly dynamic interactions with RNA, resembling FUS-WT (Figure 5A). We also prepared five glycine ALS mutations (G156E, G187S, G225V, G230C, and G399V) as an additional class of mutation to compare alongside the arginine (R) mutations. Glycines were classified as "spacers" important for controlling the fluidity of FUS condensates (Wang et al., 2018). The five G mutants displayed a range of interactions with RNA but, in general, displayed substantially more dynamic FRET fluctuations than R244C (Figures 5B and 5C). In fact, the four other R mutations (R216C, R521C, and R521G) displayed primarily static interactions, with the exception of R514G, which showed the most dynamic interaction with RNA (Figure 5C).

To calculate how dynamic the interaction is between each mutant FUS and RNA, we collected the fraction of time each molecule (>120 traces per mutant) persists in the dynamic state and plotted the population density in the form of a violin chart (Figure 5D; STAR Methods). As expected, FUS-WT is the most dynamic (median score of 0.97) (Figure 5D). The two NLS mutants and the G mutants display a wide distribution of dynamic fractions arising from traces displaying both dynamic and static FRET states. With the exception of R514G, all other R mutants show median scores clustering below 0.2, clearly indicating mostly static interactions with RNA (Figure 5D). Compared with R244C, R244K displayed dynamic FRET traces closer to FUS-WT than R244A. To further quantify the static status of each mutant, we analyzed and compiled the dwell times of the static period from over 200 smFRET traces (Figure S5B), which

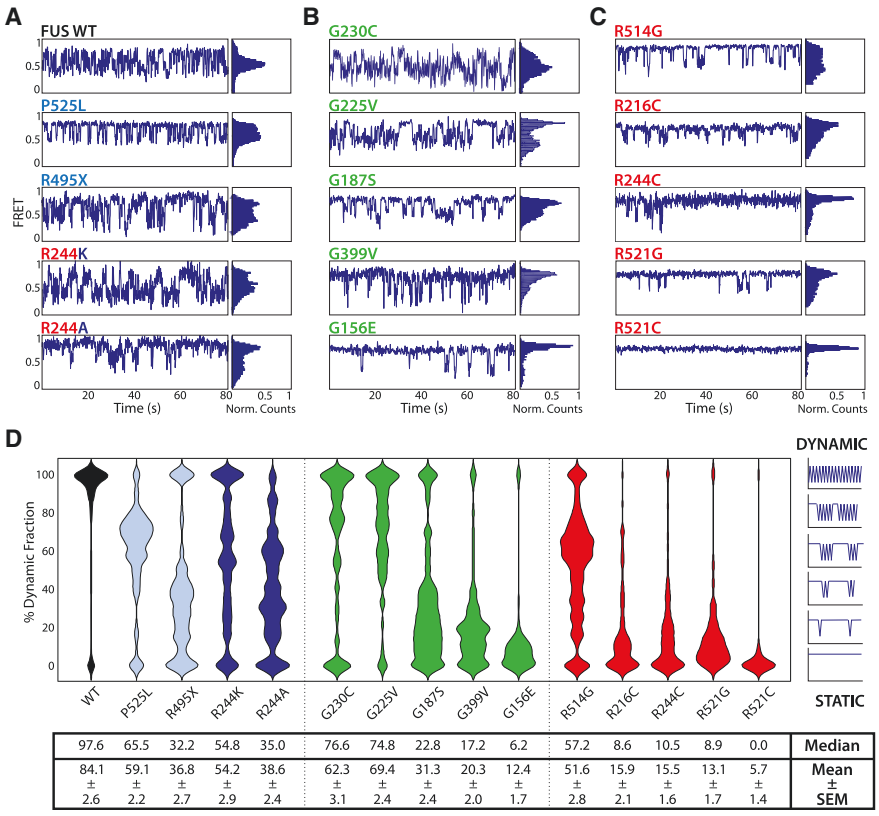

Figure 5. Arginine Mutants Induce Static RNA Interactions, whereas Other Mutants Are Comparable with the WT

(A–C) Representative FRET traces of all mutants taken at 500 nM of WT and NLS mutations (A), five ALS-linked glycine mutants (B), and five ALS-linked arginine mutants (C).

(D) Violin plot showing the population density of the fraction of time spent in the dynamic (FRET fluctuation) state for individual mutants. The dwell times were collected from over 200 events.

showed that the four most static R mutants exhibit the longest static dwell times.

EMSA analysis revealed that mutants can be divided into three categories. First, the NLS mutants and R244K exhibit a FUS-WT-like pattern of C1 shifting to C2 as the protein concentration increases (Figure S5A, class I). Second, R244A, R216C, R514G, G156E, G187S, and G225V show a pattern in which C2 appears at significantly higher protein concentrations ($\geq$250 nM), also accompanied by an aggregated smear at high concentrations (Figure S5A, class II). Third, R244C, R521G, R521C, and G399V are characterized by a persistent C1 but no C2 formation and a direct transition to high a degree of aggregation (Figure S5A, class III). Thus, at high concentrations, class I mutants mostly form C2 and display the highest level of RNA dynamics. Class III mutants, however, form an altered C1 and aggregate, corresponding to static interaction with RNA. Class II is between classes I and III; both C2 and aggregated states generate a mixture of dynamic and static FRET trajectories, respectively (Figure S5C). Taken together, the smFRET and EMSA data orthogonally support that the FUS:RNA interaction is driven by precise complex formation, with C2 the driving force for the dynamic FUS:RNA interaction, which is greatly impaired for most arginine mutants.

Glycine Mutant Droplets Exhibit Accelerated Aging, and R Mutants Become Larger Condensates

We next tested whether the altered RNA binding and increased aggregation properties of the FUS mutations affect phase separation. We used 1 μM unlabeled FUS (MBP cleaved; STAR Methods) mixed with 1 μM unlabeled U40 RNA doped with 10 nM Cy3-labeled U40, which was sufficient to induce phase separation (Figure 6A; STAR Methods). Consistent with previous studies, this result suggests that ssRNA promotes phase separation of FUS in the absence of a molecular crowding agent (Maharana et al., 2018a). The Cy3-labeled RNA was used to visualize the condensates without tagging FUS and to track RNA dynamics using fluorescence recovery after photobleaching (FRAP). The size of condensates was determined over the course of 6 h; FUS-WT, NLS, and G mutant FUS form small droplets (area, ~1.5 μm^2, R), but R mutants grow much larger (area, ~3-6 μm^2) (Figure 6B). Even after 3 h, a stark difference in droplet size can be observed (Figure 6C). This is in agreement with the EMSA results; the less dynamic and aggregation-prone R mutants formed into much larger FUS-RNA condensates than FUS variants that showed a negligible degree of aggregation on EMSA (Figure 3B; Figure S5).

Next, FRAP was performed by photobleaching the entire area of the droplets. Thus, the recovery rate reflects the degree of RNA exchange in and out of the droplet and its mobility within the droplet, both of which can indirectly indicate the fluidity of the droplets. The WT and NLS mutant FUS displays faster and almost complete recovery of fluorescence, whereas R mutants exhibit slower and incomplete recovery. Remarkably, by contrast, G mutants display much slower and severely dampened overall recovery of fluorescence (Figures 6D and 6E). To further characterize the R mutants, we measured saturation concentration (C_{sat}) by performing a condensation assay at varying protein concentrations (Wang et al., 2018). The result clearly shows a substantially lower C_{sat} for all three R mutants tested, confirming the elevated aggregation propensity for the R mutants (Figures 6F–6H). Building on the results observed above, we hypothesize that the R mutants make deficient contact with RNA, forming an altered configuration that leads to a higher aggregation propensity and supports growth to aberrantly large condensates that are less fluid. Unexpectedly, G mutants display a unique molecular pattern: they display WT-like interactions with RNA in EMSA and smFRET assays and, likewise, form condensates comparable in size with those of FUS-WT, but the condensates undergo extremely rapid aging. Together, our results point

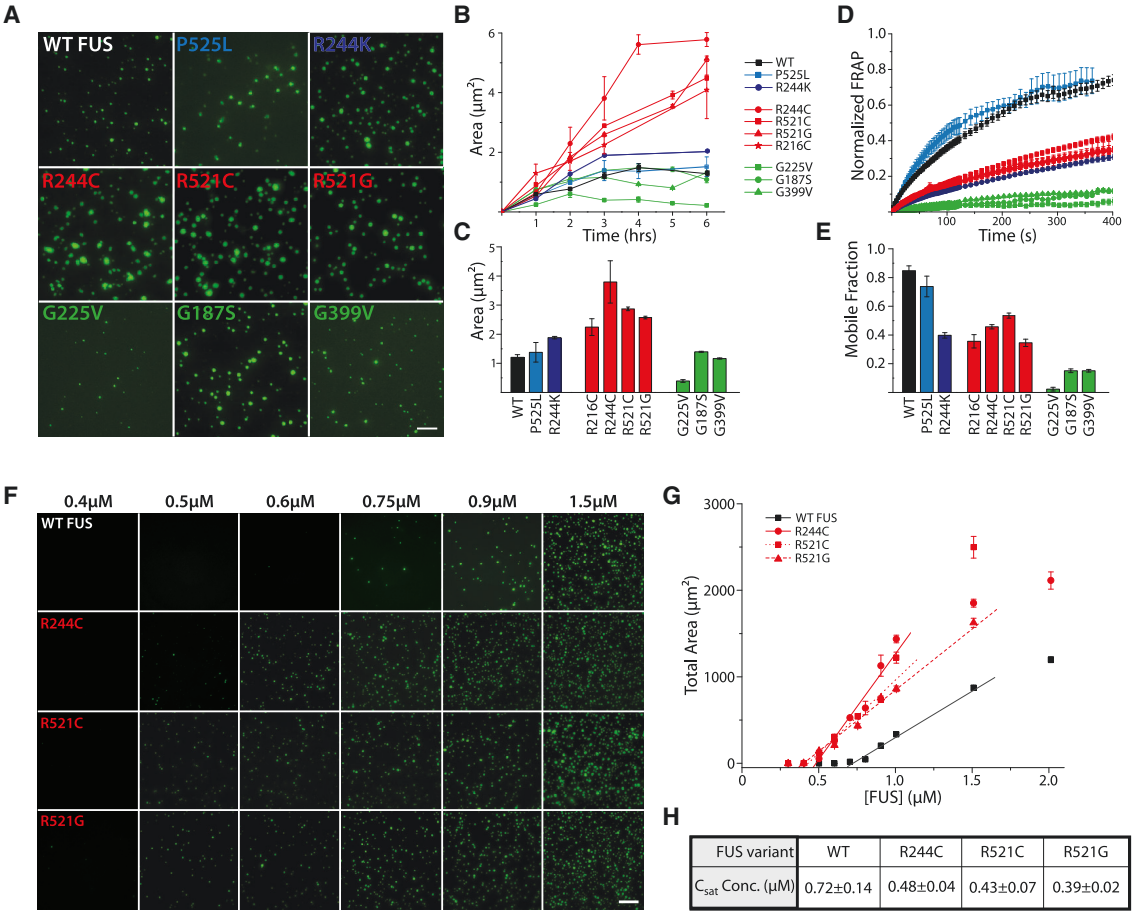

FUS variant	WT	R244C	R521C	R521G
C_{sat} Conc. (μM)	0.72±0.14	0.48±0.04	0.43±0.07	0.39±0.02

Figure 6. Arginine Mutants Form Larger Droplets, whereas Glycine Mutants Lose Fluidity Quickly

(A) Droplets formed by 1 μM FUS variants cleaved by tobacco etch virus (TEV) protease in the presence of 1 μM U40 and10 nM Cy3-labeled U40 RNA. The scale bar indicates 20 μm.

(B and C) Area of WT and FUS mutant droplets plotted over time (B) and taken at the 3-h time point (C).

(D and E) FRAP curves for FUS variants (D) and the mobile fraction after 3 h (E).

All errors bars are SEM.

(F) $C_{saturation}$ images taken for WT and R mutants.

(G) Numerical plot of $C_{saturation}$ results obtained in (F).

(H) Quantification of $C_{saturation}$ results obtained in (F).

toward disparate molecular mechanisms underlying pathogenesis, resulting from selective loss of arginine versus glycine.

Kapβ2 Rescues FUS Mutant Defects at Multiple Scales

Recent studies have reported that Kap-β2 (Kapβ2), a nuclear import receptor, plays a critical role in disaggregating FUS and FUS-related protein aggregates (Guo et al., 2018; Hofweber et al., 2018; Qamar et al., 2018; Yoshizawa et al., 2018), providing a promising new therapeutic avenue. So far, the disaggregation activity was studied only in the context of FUS condensates without RNA. Here we tested the activity of Kapβ2 in the presence of RNA. Is Kapβ2 able to reverse the defective molecular signatures of mutant FUS, including loss of the dynamic interaction with RNA, the increased aggregation propensity of the FUS:RNA complex, and the formation of larger, non-spherical FUS-RNA condensates?

First we conducted the EMSA analysis for R244C (500 nM) and pdU50 RNA (1 nM) mixed with increasing concentrations of Kapβ2. We confirmed that Kapβ2 does not bind RNA without FUS (Figure 7A, second lane). The aggregated band of R244C-bound pdU50 persists even in the presence of Kapβ2 in concentrations below that of R244C (500 nM). At an equimolar concentration of Kapβ2 (500 nM), the aggregated band is substantially diminished and completely abolished at even higher concentrations, indicating clear FUS-RNA disaggregating activity by Kapβ2. Interestingly, the FUS-RNA C1 band is maintained across Kapβ2 concentrations, suggesting that Kapβ2 does not compete with RNA binding to a significant degree. The same EMSA assay performed with the most aggregation-prone G mutant, G156E, also showed a similar Kapβ2 dissolution effect, albeit at a higher Kapβ2 concentration (Figure S6B). Again, Kapβ2 did not noticeably disrupt G156E-RNA interaction. This

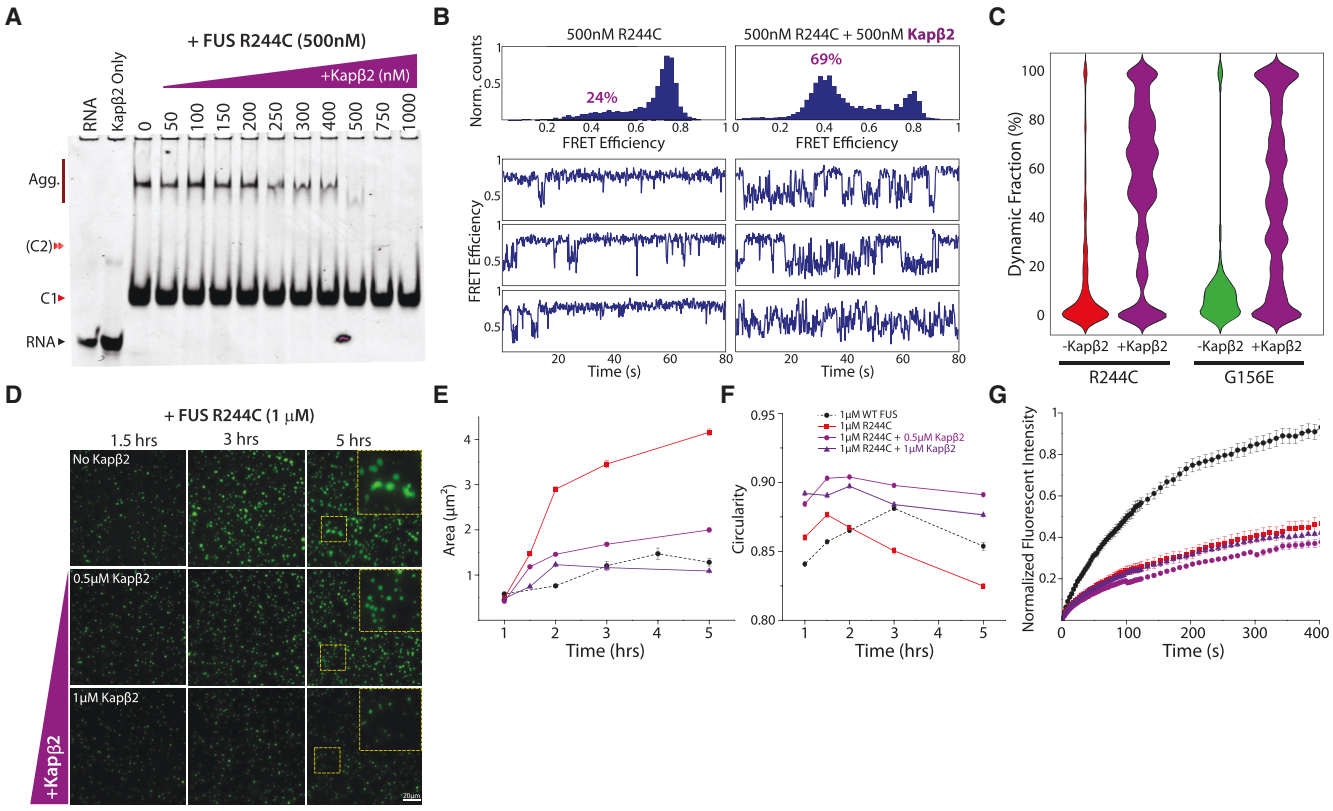

Figure 7. Kapβ2 Induced Recovery

(A) EMSA gel of 500 nM R244C incubated with titrating concentrations of Kapβ2 (0–1,000 nM).

(B) Representative FRET traces and FRET histograms of 500 nM R244C in the absence and presence of equimolar concentrations of Kapβ2.

(C) Violin plot of the fraction of dynamic molecules observed in smFRET traces.

(D) Droplets formed using 1 μM R244C in the absence and presence of 0.5 and 1 μM Kapβ2 over time.

(E) Quantification of the size of condensates.

(F) Plot of circularity of each droplet condition over time.

(G) Initial FRAP curves of the droplets at 3 h.

All error bars are SEM.

result reveals that Kapβ2 selectively dissolves aggregated FUS bound to RNA without disrupting FUS-RNA interaction.

Second, we tested the R244C-RNA interaction using our smFRET in the absence and presence of Kapβ2. The high FRET peak for R244C (500 nM) was accompanied by predominantly static smFRET traces (Figure 7B, left panel). Strikingly, addition of equimolar Kapβ2 (500 nM) induced the appearance of a broad mid-FRET peak accompanied by highly dynamic FRET fluctuations in a significant fraction of smFRET traces, suggesting recovery of WT-RNA-like interactions by Kapβ2 (Figures 7B and 7C). Consistently, G156E showed the same increase in dynamics upon addition of Kapβ2, albeit to a lesser extent, as evidenced by a smaller mid-FRET peak (Figure S6C). Because Kapβ2 does not interact with RNA by itself, such rescue can only arise from Kapβ2 interacting with FUS to directly dissolve aggregates, which is sufficient for recovering the WT-like dynamics of the FUS-RNA interaction. Rescue of FUS mutant dynamics by Kapβ2, however, is not complete because a small fraction of high-FRET peak remains, which we relate to the less fluid condensate discussed below.

Third, we performed a R244C-RNA phase separation assay in the absence and presence of Kapβ2. As before, R244C-RNA formed into large, aberrantly shaped condensates in the absence of Kapβ2. When 0.5–1 μM Kapβ2 was added, the condensates were significantly smaller in size and more circular in shape, reflecting recovery to the level of WT FUS over the course of 5 h (Figures 7D–7F). Interestingly, FRAP analysis showed that the remaining R244C droplets are just as solid-like as the R244C condensates without Kapβ2 (Figure 7G). This is in contrast to the WT condensates, which dissolved completely when mixed with Kapβ2 (Figure S6D). Kapβ2 addition to G156E-RNA condensate substantially reduced the droplet size but left behind fiber-like structures (Figure S6E). The small but non-fluid condensates of R244C and G156E suggest that Kapβ2 does dissolve mutant RNP condensates but is unable to fully resolve a solid-like component of the mutant droplet. This is likely related to the small fraction of molecules trapped in the high FRET peak shown above (Figures 7B and S6C).

Here we demonstrate that Kapβ2 reverses FUS mutants' behavioral defects by dissolving protein-RNA aggregates while

enabling proper and dynamic FUS-RNA interaction (via EMSA and smFRET). Furthermore, addition of Kapβ2 to mutant RNP condensates revealed that these may be heterogeneous structures consisting of one component that is capable of interacting with Kapβ2 and another component that is recalcitrant to Kapβ2's activity.

DISCUSSION

The Initial Seeding Is Defective in Arginine Mutants

FUS is a nuclear RBP involved in many steps of RNA metabolism. Because of its functions in transcription (Rabbitts et al., 1993; Yang et al., 2014), mRNA splicing (Sun et al., 2015; Zhou et al., 2013), and microRNA processes (Dini Modigliani et al., 2014; Morlando et al., 2012; Zhang et al., 2018), its RNA-binding property is a critical parameter to consider when studying FUS function and phase separation. Previous studies have shown that the high RNA-to-protein ratio in the nucleus buffers phase separation of FUS despite the high concentration of FUS. Accordingly, microinjection of RNase into cell nuclei induces rapid condensation of GFP-labeled FUS proteins (Maharana et al., 2018a), strongly demonstrating that RNA keeps FUS in a soluble state in the nucleus. We used smFRET to examine how FUS changes the conformation of the flexible chain of an RNA substrate. Our result demonstrates that a monomeric FUS establishes a stable interaction with ssRNA by wrapping it around the protein (i.e., a steady high FRET signal) (Figure 1). Real-time flow measurements showed that such monomer FUS binding to RNA involves a clear two-step process. FUS makes extensive contact with RNA (Yoshizawa et al., 2018), and the two steps may represent the C-terminal RNA binding domain making the initial contact with RNA, followed by a conformational change in FUS that makes a secondary contact that wraps RNA. Strikingly, such two-step binding is abolished for the ALS-linked R244C mutant, which exhibits extremely slow and poorly defined binding (Figure 4). Such defective binding of a single arginine point mutation is likely to have functional consequences in the nucleus, where its primary roles involve RNA binding. Furthermore, the defective monomeric state remains as is (C1 in the EMSA gel; Figure 3B) or leads to higher order complex of RNP aggregates in lieu of the formation of the dynamic C2 state seen in FUS-WT. Therefore, we interpret C1 (the monomer-bound high FRET state) as a critical step required for proper C2 formation, which exhibits dynamic interactions with RNA.

RNA Is a Multivalent Platform, and Multimer FUS Induces Dynamic Interaction with RNA

We demonstrate that RNA length controls the valency of FUS, consistent with previous findings (Schwartz et al., 2013; Weber and Brangwynne, 2012). RNA length-dependent FUS binding reveals that 10–30, 40–50, and 70 nt of ssRNA can accommodate up to one (C1), two (C2), and three units (C3) of FUS, respectively (Figure 2C), suggesting that a monomer occupies ~20–25 nt. Importantly, the C1 state involves a high degree of RNA compaction by FUS, as evident from the same position of C1 bands on EMSA gels despite different lengths of RNA. In contrast, the C2 and C3 states both induce highly dynamic interactions with RNA (Figure 2B). It is noteworthy that FUS, which binds ssRNA with nanomolar affinity (based on our EMSA analysis), is present at a concentration of 2–3 μM in cells (Maharana et al., 2018a). The emerging view is that the long cellular mRNA can be targeted by multimers of FUS inducing highly dynamic interactions with the cellular RNA. In the cytoplasm where the RNA-to-protein ratio is low, such dynamic, multivalent protein-RNA interactions can also lead to coalescence into RNP condensates.

We envision that proper RNP condensation entails two sequential steps: the initial protein-RNA interaction and the subsequent RNP-RNP interaction mediated by protein-protein contact. Our results obtained for the WT FUS reflect that multimer (C2)-induced dynamic FUS-RNA interaction is the proper protein-RNA format that supports the subsequent FUS-RNA:FUS-RNA interaction that leads to LLPS. Strikingly, the majority of R mutants exhibited loss of such a multimer-induced dynamic FUS-RNA interaction (Figures 3 and 5), emphasizing the pivotal role of arginine residues in enabling the proper RNA-protein contact required for proper C2 formation. In contrast, the G mutants are competent for multimer-induced FUS-RNA interaction but condense into non-fluid droplets. This reveals that glycine makes less of a contribution to FUS-RNA interaction but more to RNP-RNP or protein-protein interaction.

NLS, R, and G Mutants Display Disparate Molecular Phenotypes

We examined a total of 15 versions of FUS proteins: WT FUS and 12 ALS/FTD-linked FUS mutations with two control R mutants. Despite the severe pathogenic nature of the two NLS mutants, our results reveal that they are comparable with the WT FUS in every aspect with regard to RNA binding (Figure S5), including multimer-induced dynamics (Figure 5) and the formation of normal-sized fluid condensates (Figure 6). This result reiterates the significance of the NLS domain, which, when mutated, can disrupt nuclear transport, leading to advanced disease onset, albeit through a distinct molecular mechanism compared with IDR-clustered ALS mutations (Guo et al., 2018; Hofweber et al., 2018; Qamar et al., 2018; Yoshizawa et al., 2018). Based on our findings, the R mutants interact statically with RNA, arising from the formation of a defective C1 that gives rise to aggregated RNP complexes and large and noncircular condensate. The two control mutants, R244K and R244A, strongly suggest that R244C's molecular defects are due to the loss of arginine.

At first glance, our results may appear to contradict a recently published report (Wang et al., 2018) that defined the role of arginines, which were classified as "stickers" in increasing the propensity for phase separation, whereas loss of arginine in our results increased the aggregation potential. However, there are two major differences. The previous study mutated many arginines (10–40) simultaneously, which increased the C_{sat} (the threshold concentration to induce phase separation), and that study was conducted in the absence of RNA. Here we investigated the effect of a single arginine mutation in the presence of RNA. Taken together, the overall high density of arginine is critical for promoting protein condensation, whereas individual arginines may be important for establishing proper contacts with RNA, allowing the formation of fluid condensates. We predict

that the molecular deficiency of the R mutants will affect their RNA-binding functions in the nucleus. However, the G mutants exhibit a unique pattern of WT-like dynamic interaction with RNA on a single-molecule level but extreme loss of fluidity in condensates. Unlike the R mutant case, the characteristic of glycine mutants are in agreement with the predicted molecular grammar of glycine as a spacer, enhancing fluidity (Wang et al., 2018). Our study demonstrates that removing even a single glycine can drastically affect the fluidity of FUS-RNA condensate, emphasizing the critical role of every glycine in driving fluid RNP condensation. Based on our molecular probing, the G mutations may not reduce FUS activity in the nucleus, where protein-RNA interaction dominates, but may drive formation of gel/solid-like condensates in the cytoplasm, where RNA concentrations are low and the protein's phase separation propensity is amplified (Maharana et al., 2018a). The solid-like condensates may also accelerate disease progression and dampen disaggregation potential by other proteins.

Kapβ2 Reverses the Molecular Defect of R and G Mutants

The recent studies that led to the discovery that Kap-β2 can act as a protein disaggregase (Guo et al., 2018; Hofweber et al., 2018; Qamar et al., 2018; Yoshizawa et al., 2018) have sparked interest in the potential application of such proteins as treatment for incurable neurodegenerative diseases. Our recent study showed that ubiquillin-2, which physically associates with FUS in cells, is capable of relaxing static mutant FUS-RNA interactions and promoting fluid condensate formation (Alexander et al., 2018). Here we demonstrate that Kapβ2 rescues the mutants' defective interactions with RNA by reviving the dynamic FUS-RNA interaction in both mutants. The Kapβ2-induced increase in dynamics was more pronounced in the R mutants than in the G mutants, based on the fraction of molecules in the mid-FRET peak, which is further quantified in a violin plot (Figure 7). One puzzling observation is that there is no C2 formation for R244C+Kap-β2 despite the distinct appearance of mid-FRET peak accompanied by FRET fluctuations. One possibility is that the dynamic FRET fluctuation arises from the FUS-Kapβ2 complex interacting with RNA, but this requires further probing of the molecular mechanism.

Kapβ2 led to formation of smaller droplets in both R and G mutants, suggesting that Kapβ2 interaction prevents aberrant accumulation of aggregates that eventually result in larger condensates. Nonetheless, compared with the FUS-RNA droplets formed by WT protein that were dissolved completely by Kapβ2, both R and G mutant condensates remained as small but non-fluid condensates or fibrous solids, respectively (Figure 7). Such undissolved aggregates are consistent with the small fraction of the high FRET peak persisting even after Kapβ2 addition. This result reveals that the rescue effect of Kapβ2 may not be equivalent in all FUS mutant molecules or in the types of FUS aggregates that form. Our future efforts will be directed to elucidating the mechanistic basis of the Kapβ2 rescue effect on FUS-RNA interaction. It will also be critical to probe FUS variants with non-ALS/FTD-linked mutations to see whether the molecular phenotypes that we observed are due to the specific positions of R and G or simply due to the type of amino acid substitutions.

STAR★METHODS

Detailed methods are provided in the online version of this paper and include the following:

- KEY RESOURCES TABLE
- LEAD CONTACT AND MATERIALS AVAILABILITY
- METHOD DETAILS
  - Preparation of WT FUS, FUS mutants, and RNA constructs
  - Characterization of WT FUS and FUS mutants
- QUANTIFICATION AND STATISTICAL ANALYSIS
  - Single molecule FRET and PIFE
  - EMSA gel quantification
  - Phase separation and C saturation
  - FRAP analysis
  - Fluorescent Anisotropy
- DATA AND CODE AVAILABILITY

SUPPLEMENTAL INFORMATION

Supplemental Information can be found online at https://doi.org/10.1016/j.molcel.2019.09.022.

ACKNOWLEDGMENTS

We thank the members of the Sua Myong and Taekjip Ha laboratory for helpful discussions. This project was supported by a Catalyst Research Award and Discovery Award from Johns Hopkins University and the National Institute of Neurodegeneration and Stroke, National Alzheimer's Project Act (NAPA) 1-RF1-NS113636-01 for all members at Johns Hopkins University, National Science Foundation Physics Frontiers Center Program 0822613 through the Center for the Physics of Living Cells (to A.G.N. and S.M.), and 1F31GM134641–01 to V.V. and 5T32GM007231–45 to K.R. and V.V. We also acknowledge an EMF/AFAR fellowship (to L.G.), an AARF fellowship (to L.G.), a Target ALS Springboard Fellowship (to L.G.), NIH grant T32GM008275 (to C.M.F.), NIH grant R21NS090205 (to J. Shorter), The G. Harold and Leila Y. Mathers Charitable Foundation (to J. Shorter), Target ALS (to J. Shorter), ALSA (to J. Shorter), and the Packard Center for ALS Research (to J. Shorter).

AUTHOR CONTRIBUTIONS

A.G.N., J. Sarkar, X.C., and K.R. performed the majority of the experiments. V.V., B.G., M.H., and J.C.L. contributed by performing several FUS mutant characterizations and H.R.K. by offering help with setting up FRAP. L.G., C.M.F., and J. Shorter prepared and provided Kapryopherin-β2. A.G.N., J. Sarkar, and S.M. wrote and K.R., L.G., and C.M.F. edited the manuscript.

DECLARATION OF INTERESTS

The authors declare no competing interests.

Received: June 21, 2019
Revised: August 19, 2019
Accepted: September 20, 2019
Published: October 17, 2019

REFERENCES

Alexander, E.J., Ghanbari Niaki, A., Zhang, T., Sarkar, J., Liu, Y., Nirujogi, R.S., Pandey, A., Myong, S., and Wang, J. (2018). Ubiquilin 2 modulates ALS/FTD-linked FUS-RNA complex dynamics and stress granule formation. Proc. Natl. Acad. Sci. USA *115*, E11485–E11494.

Aulas, A., and Vande Velde, C. (2015). Alterations in stress granule dynamics driven by TDP-43 and FUS: a link to pathological inclusions in ALS? Front. Cell. Neurosci. *9*, 423.

Bosco, D.A., Lemay, N., Ko, H.K., Zhou, H., Burke, C., Kwiatkowski, T.J., Jr., Sapp, P., McKenna-Yasek, D., Brown, R.H., Jr., and Hayward, L.J. (2010). Mutant FUS proteins that cause amyotrophic lateral sclerosis incorporate into stress granules. Hum. Mol. Genet. *19*, 4160–4175.

Burke, K.A., Janke, A.M., Rhine, C.L., and Fawzi, N.L. (2015). Residue-by-Residue View of In Vitro FUS Granules that Bind the C-Terminal Domain of RNA Polymerase II. Mol. Cell *60*, 231–241.

Daigle, J.G., Lanson, N.A., Jr., Smith, R.B., Casci, I., Maltare, A., Monaghan, J., Nichols, C.D., Kryndushkin, D., Shewmaker, F., and Pandey, U.B. (2013). RNA-binding ability of FUS regulates neurodegeneration, cytoplasmic mislocalization and incorporation into stress granules associated with FUS carrying ALS-linked mutations. Hum. Mol. Genet. *22*, 1193–1205.

Dini Modigliani, S., Morlando, M., Errichelli, L., Sabatelli, M., and Bozzoni, I. (2014). An ALS-associated mutation in the FUS 3′-UTR disrupts a microRNA-FUS regulatory circuitry. Nat. Commun. *5*, 4335.

Dormann, D., Rodde, R., Edbauer, D., Bentmann, E., Fischer, I., Hruscha, A., Than, M.E., Mackenzie, I.R., Capell, A., Schmid, B., et al. (2010). ALS-associated fused in sarcoma (FUS) mutations disrupt Transportin-mediated nuclear import. EMBO J. *29*, 2841–2857.

Elbaum-Garfinkle, S., Kim, Y., Szczepaniak, K., Chen, C.C., Eckmann, C.R., Myong, S., and Brangwynne, C.P. (2015). The disordered P granule protein LAF-1 drives phase separation into droplets with tunable viscosity and dynamics. Proc. Natl. Acad. Sci. USA *112*, 7189–7194.

Guo, L., and Shorter, J. (2015). It's Raining Liquids: RNA Tunes Viscoelasticity and Dynamics of Membraneless Organelles. Mol. Cell *60*, 189–192.

Guo, L., Kim, H.J., Wang, H., Monaghan, J., Freyermuth, F., Sung, J.C., O'Donovan, K., Fare, C.M., Diaz, Z., Singh, N., et al. (2018). Nuclear-Import Receptors Reverse Aberrant Phase Transitions of RNA-Binding Proteins with Prion-like Domains. Cell *173*, 677–692.e20.

Hofweber, M., Hutten, S., Bourgeois, B., Spreitzer, E., Niedner-Boblenz, A., Schifferer, M., Ruepp, M.D., Simons, M., Niessing, D., Madl, T., et al. (2018). Phase Separation of FUS Is Suppressed by Its Nuclear Import Receptor and Arginine Methylation. Cell *173*, 706–719.e13.

Hwang, H., and Myong, S. (2014). Protein induced fluorescence enhancement (PIFE) for probing protein-nucleic acid interactions. Chem. Soc. Rev. *43*, 1221–1229.

Hwang, H., Kim, H., and Myong, S. (2011). Protein induced fluorescence enhancement as a single molecule assay with short distance sensitivity. Proc. Natl. Acad. Sci. USA *108*, 7414–7418.

Hyman, A.A., Weber, C.A., and Jülicher, F. (2014). Liquid-liquid phase separation in biology. Annu. Rev. Cell Dev. Biol. *30*, 39–58.

Jain, A., and Vale, R.D. (2017). RNA phase transitions in repeat expansion disorders. Nature *546*, 243–247.

Kang, J., Lim, L., and Song, J. (2018). ATP enhances at low concentrations but dissolves at high concentrations liquid-liquid phase separation (LLPS) of ALS/FTD-causing FUS. Biochem. Biophys. Res. Commun. *504*, 545–551.

Kapeli, K., Martinez, F.J., and Yeo, G.W. (2017). Genetic mutations in RNA-binding proteins and their roles in ALS. Hum. Genet. *136*, 1193–1214.

Kim, Y., and Myong, S. (2016). RNA Remodeling Activity of DEAD Box Proteins Tuned by Protein Concentration, RNA Length, and ATP. Mol. Cell *63*, 865–876.

Koh, H.R., Xing, L., Kleiman, L., and Myong, S. (2014). Repetitive RNA unwinding by RNA helicase A facilitates RNA annealing. Nucleic Acids Res. *42*, 8556–8564.

Kwiatkowski, T.J., Jr., Bosco, D.A., Leclerc, A.L., Tamrazian, E., Vanderburg, C.R., Russ, C., Davis, A., Gilchrist, J., Kasarskis, E.J., Munsat, T., et al. (2009). Mutations in the FUS/TLS gene on chromosome 16 cause familial amyotrophic lateral sclerosis. Science *323*, 1205–1208.

Lagier-Tourenne, C., Polymenidou, M., and Cleveland, D.W. (2010). TDP-43 and FUS/TLS: emerging roles in RNA processing and neurodegeneration. Hum. Mol. Genet. *19* (R1), R46–R64.

Lagier-Tourenne, C., Polymenidou, M., Hutt, K.R., Vu, A.Q., Baughn, M., Huelga, S.C., Clutario, K.M., Ling, S.C., Liang, T.Y., Mazur, C., et al. (2012). Divergent roles of ALS-linked proteins FUS/TLS and TDP-43 intersect in processing long pre-mRNAs. Nat. Neurosci. *15*, 1488–1497.

Langdon, E.M., Qiu, Y., Ghanbari Niaki, A., McLaughlin, G.A., Weidmann, C.A., Gerbich, T.M., Smith, J.A., Crutchley, J.M., Termini, C.M., Weeks, K.M., et al. (2018). mRNA structure determines specificity of a polyQ-driven phase separation. Science *360*, 922–927.

Li, Y.R., King, O.D., Shorter, J., and Gitler, A.D. (2013). Stress granules as crucibles of ALS pathogenesis. J. Cell Biol. *201*, 361–372.

Lin, Y., Protter, D.S., Rosen, M.K., and Parker, R. (2015). Formation and Maturation of Phase-Separated Liquid Droplets by RNA-Binding Proteins. Mol. Cell *60*, 208–219.

Ling, S.C., Polymenidou, M., and Cleveland, D.W. (2013). Converging mechanisms in ALS and FTD: disrupted RNA and protein homeostasis. Neuron *79*, 416–438.

Mackenzie, I.R.A., and Neumann, M. (2017). Fused in Sarcoma Neuropathology in Neurodegenerative Disease. Cold Spring Harb. Perspect. Med. *7*, a024299.

Maharana, S., Wang, J., Papadopoulos, D.K., Richter, D., Pozniakovsky, A., Poser, I., Bickle, M., Rizk, S., Guillén-Boixet, J., Franzmann, T.M., et al. (2018a). RNA buffers the phase separation behavior of prion-like RNA binding proteins. Science *360*, 918–921.

Molliex, A., Temirov, J., Lee, J., Coughlin, M., Kanagaraj, A.P., Kim, H.J., Mittag, T., and Taylor, J.P. (2015). Phase separation by low complexity domains promotes stress granule assembly and drives pathological fibrillization. Cell *163*, 123–133.

Morlando, M., Dini Modigliani, S., Torrelli, G., Rosa, A., Di Carlo, V., Caffarelli, E., and Bozzoni, I. (2012). FUS stimulates microRNA biogenesis by facilitating co-transcriptional Drosha recruitment. EMBO J. *31*, 4502–4510.

Nolan, M., Talbot, K., and Ansorge, O. (2016). Pathogenesis of FUS-associated ALS and FTD: insights from rodent models. Acta Neuropathol. Commun. *4*, 99.

Nomura, T., Watanabe, S., Kaneko, K., Yamanaka, K., Nukina, N., and Furukawa, Y. (2014). Intranuclear aggregation of mutant FUS/TLS as a molecular pathomechanism of amyotrophic lateral sclerosis. J. Biol. Chem. *289*, 1192–1202.

Patel, A., Lee, H.O., Jawerth, L., Maharana, S., Jahnel, M., Hein, M.Y., Stoynov, S., Mahamid, J., Saha, S., Franzmann, T.M., et al. (2015). A Liquid-to-Solid Phase Transition of the ALS Protein FUS Accelerated by Disease Mutation. Cell *162*, 1066–1077.

Protter, D.S.W., and Parker, R. (2016). Principles and Properties of Stress Granules. Trends Cell Biol. *26*, 668–679.

Qamar, S., Wang, G., Randle, S.J., Ruggeri, F.S., Varela, J.A., Lin, J.Q., Phillips, E.C., Miyashita, A., Williams, D., Strohl, F., et al. (2018). FUS Phase Separation Is Modulated by a Molecular Chaperone and Methylation of Arginine Cation-pi Interactions. Cell *173*, 720–734.e15.

Qiu, Y., Antony, E., Doganay, S., Koh, H.R., Lohman, T.M., and Myong, S. (2013). Srs2 prevents Rad51 filament formation by repetitive motion on DNA. Nat. Commun. *4*, 2281.

Rabbitts, T.H., Forster, A., Larson, R., and Nathan, P. (1993). Fusion of the dominant negative transcription regulator CHOP with a novel gene FUS by translocation t(12;16) in malignant liposarcoma. Nat. Genet. *4*, 175–180.

Schwartz, J.C., Wang, X., Podell, E.R., and Cech, T.R. (2013). RNA seeds higher-order assembly of FUS protein. Cell Rep. *5*, 918–925.

Stoica, R., Paillusson, S., Gomez-Suaga, P., Mitchell, J.C., Lau, D.H., Gray, E.H., Sancho, R.M., Vizcay-Barrena, G., De Vos, K.J., Shaw, C.E., et al. (2016). ALS/FTD-associated FUS activates GSK-3β to disrupt the VAPB-PTPIP51 interaction and ER-mitochondria associations. EMBO Rep. *17*, 1326–1342.

Sun, S., Ling, S.C., Qiu, J., Albuquerque, C.P., Zhou, Y., Tokunaga, S., Li, H., Qiu, H., Bui, A., Yeo, G.W., et al. (2015). ALS-causative mutations in FUS/TLS

confer gain and loss of function by altered association with SMN and U1-snRNP. Nat. Commun. *6*, 6171.

Svetoni, F., Frisone, P., and Paronetto, M.P. (2016). Role of FET proteins in neurodegenerative disorders. RNA Biol. *13*, 1089–1102.

Van Treeck, B., Protter, D.S.W., Matheny, T., Khong, A., Link, C.D., and Parker, R. (2018). RNA self-assembly contributes to stress granule formation and defining the stress granule transcriptome. Proc. Natl. Acad. Sci. USA *115*, 2734–2739.

Vance, C., Rogelj, B., Hortobágyi, T., De Vos, K.J., Nishimura, A.L., Sreedharan, J., Hu, X., Smith, B., Ruddy, D., Wright, P., et al. (2009). Mutations in FUS, an RNA processing protein, cause familial amyotrophic lateral sclerosis type 6. Science *323*, 1208–1211.

Wang, W.Y., Pan, L., Su, S.C., Quinn, E.J., Sasaki, M., Jimenez, J.C., Mackenzie, I.R., Huang, E.J., and Tsai, L.H. (2013). Interaction of FUS and HDAC1 regulates DNA damage response and repair in neurons. Nat. Neurosci. *16*, 1383–1391.

Wang, X., Schwartz, J.C., and Cech, T.R. (2015). Nucleic acid-binding specificity of human FUS protein. Nucleic Acids Res. *43*, 7535–7543.

Wang, J., Choi, J.M., Holehouse, A.S., Lee, H.O., Zhang, X., Jahnel, M., Maharana, S., Lemaitre, R., Pozniakovsky, A., Drechsel, D., et al. (2018). A Molecular Grammar Governing the Driving Forces for Phase Separation of Prion-like RNA Binding Proteins. Cell *174*, 688–699.e16.

Weber, S.C., and Brangwynne, C.P. (2012). Getting RNA and protein in phase. Cell *149*, 1188–1191.

Yang, L., Gal, J., Chen, J., and Zhu, H. (2014). Self-assembled FUS binds active chromatin and regulates gene transcription. Proc. Natl. Acad. Sci. USA *111*, 17809–17814.

Yoshizawa, T., Ali, R., Jiou, J., Fung, H.Y.J., Burke, K.A., Kim, S.J., Lin, Y., Peeples, W.B., Saltzberg, D., Soniat, M., et al. (2018). Nuclear Import Receptor Inhibits Phase Separation of FUS through Binding to Multiple Sites. Cell *173*, 693–705 e22.

Zhang, H., Elbaum-Garfinkle, S., Langdon, E.M., Taylor, N., Occhipinti, P., Bridges, A.A., Brangwynne, C.P., and Gladfelter, A.S. (2015). RNA Controls PolyQ Protein Phase Transitions. Mol. Cell *60*, 220–230.

Zhang, T., Wu, Y.C., Mullane, P., Ji, Y.J., Liu, H., He, L., Arora, A., Hwang, H.Y., Alessi, A.F., Niaki, A.G., et al. (2018). FUS Regulates Activity of MicroRNA-Mediated Gene Silencing. Mol. Cell *69*, 787–801 e8.

Zhou, Y., Liu, S., Liu, G., Oztürk, A., and Hicks, G.G. (2013). ALS-associated FUS mutations result in compromised FUS alternative splicing and autoregulation. PLoS Genet. *9*, e1003895.

STAR★METHODS

KEY RESOURCES TABLE

REAGENT or RESOURCE	SOURCE	IDENTIFIER
Antibodies		
Anti-GFP (RABBIT) Antibody Biotin Conjugated	Rockland Antibodies & Assays	600-406-215; RRID:AB_10796022
Bacterial and Virus Strains		
E. Coli BL21(DE3) Chemically Competent Cells	Millipore Sigma	CMC0014-20X40UL
Chemicals, Peptides, and Recombinant Proteins		
AcTEV Protease	Fisher Scientific	Cat #: 12-575-015
Ribonuclease A from bovine pancreas	Millipore Sigma	R6513
cOmplete Protease Inhibitor Cocktail	Roche	11697498001
Glucose Oxidase from Aspergillus niger	Sigma-Aldrich	G2133
Catalase from bovine liver	Sigma-Aldrich	C3155
IGEPAL® CA-630	Sigma-Aldrich	I8896
HisTrap FF Crude, 5 ml	GE Healthcare	17528601
Cy3 NHS Ester	GE Healthcare	PA13101
Cy5 NHS Ester	GE Healthcare	PA15100
Oligonucleotides		
Biotin-18-mer: 5′- /biotin/rUrGrG rCrGrA rCrGrG rCrArG rCrGrA rGrGrC/3AmMO/ −3′	IDT	N/A
U10-18-mer: 5′- /5AmMC6/rUrUrU rUrUrU rUrUrU rUrGrC rCrUrC rGrCrU rGrCrC rGrUrC rGrCrC rA −3′	IDT	N/A
U20-18-mer: 5′- /5AmMC6/rUrUrU rUrUrU rUrUrU rUrUrU rUrUrU rUrUrU rUrUrG rCrCrU rCrGrC rUrGrC rCrGrU rCrGrC rCrA −3′	IDT	N/A
U30-18-mer: 5′- /5AmMC6/rUrUrU rUrUrU rUrUrU rUrUrU rUrUrU rUrUrU rUrUrU rUrUU rUrUrU rGrCrC rUrCrG rCrUrG rCrCrG rUrCrG rCrCrA −3′	IDT	N/A
U40-18-mer: 5′- /5AmMC6/rUrUrU rUrUrU rUrUrU rUrUrU rUrUrU rUrUrU rUrUrU rUrUrU rUrUrU rUrUrU rUrUrU rUrUrU rUrGrC rCrUrC rGrCrU rGrCrC rGrUrC rGrCrC rA −3′	IDT	N/A
U50-18-mer: 5′- /5AmMC6/rUrUrU rUrUrU rUrUrU rUrUrU rUrUrU rUrUrU rUrUrU rUrUrU rUrUrU rUrUrU rUrUrU rUrUrU rUrUrU rUrUrU rUrUrU rUrUrG rCrCrU rCrGrC rUrGrC rCrGrU rCrGrC rCrA −3′	IDT	N/A
U70-18-mer: 5′- /5AmMC6/rUrUrU rUrUrU rUrUrU rUrUrU rUrUrU rUrUrU rUrUrU rUrUrU rUrUrU rUrUrU rUrUrU rUrUrUr UrUrU rUrUrU rUrUrU rUrUrU rUrUrU rUrUrU rUrUrU rUrUrU rUrUrU rUrUrU rUrGrC rCrUrC rGrCrU rGrCrC rGrUrC rGrCrC rA −3′	IDT	N/A
U40: 5′- rUrUrU rUrUrU rUrUrU rUrUrU rUrUrU rUrUrU rUrUrU rUrUrU rUrUrU rUrUrU rUrUrU rUrUrU rU/3AmMO/ −3′	IDT	N/A
Recombinant DNA		
pTHMT/FUS$_{WT}$ (encoding 6xHis-MBP-FUSWT)	GenScript	N/A
pTHMT/FUS$_{P525L}$ (encoding 6xHis-MBP-FUSP525L)	GenScript	N/A
pTHMT/FUS$_{R495X}$ (encoding 6xHis-MBP-FUSR495X)	GenScript	N/A
pTHMT/FUS$_{R244C}$ (encoding 6xHis-MBP-FUSR244C)	GenScript	N/A
pTHMT/FUS$_{R244K}$ (encoding 6xHis-MBP-FUSR244K)	GenScript	N/A
pTHMT/FUS$_{R244A}$ (encoding 6xHis-MBP-FUSR244A)	GenScript	N/A
pTHMT/FUS$_{R514G}$ (encoding 6xHis-MBP-FUSR514G)	GenScript	N/A

(*Continued on next page*)

Continued

REAGENT or RESOURCE	SOURCE	IDENTIFIER
pTHMT/FUS$_{R216C}$ (encoding 6xHis-MBP-FUSR216C)	GenScript	N/A
pTHMT/FUS$_{R521G}$ (encoding 6xHis-MBP-FUSR521G)	GenScript	N/A
pTHMT/FUS$_{R521C}$ (encoding 6xHis-MBP-FUSR521C)	GenScript	N/A
pTHMT/FUS$_{G230C}$ (encoding 6xHis-MBP-FUSG230C)	GenScript	N/A
pTHMT/FUS$_{G225V}$ (encoding 6xHis-MBP-FUSG225V)	GenScript	N/A
pTHMT/FUS$_{G156E}$ (encoding 6xHis-MBP-FUSG156E)	GenScript	N/A
pTHMT/FUS$_{G187S}$ (encoding 6xHis-MBP-FUSG187S)	GenScript	N/A
pTHMT/FUS$_{G399V}$(encoding 6xHis-MBP-FUSG399V)	GenScript	N/A
pTHMT/FUS$_{WT}$-EGFP (encoding 6xHis-MBP-FUSWT-EGFP)	GenScript	N/A
Software and Algorithms		
MATLAB and IDL scripts	https://physics.illinois.edu/cplc/software/	N/A
NIS-Elements Ar package	Nikon Inc.	N/A
Other		
Nunc Lab-Tek Chambered Coverglass	Thermo Scientific	155361
DNA Retardation Gels (6%)	Invitrogen	EC63655BOX
Amicon Ultra-0.5 Centrifugal Filter Unit	Millipore	UFC501096

LEAD CONTACT AND MATERIALS AVAILABILITY

Further information and requests for resources and reagents should be directed to and will be fulfilled by the Lead Contact, Sua Myong (smyong@jhu.edu).

All unique reagents generated in this study are available from the Lead Contact without restriction.

METHOD DETAILS

Preparation of WT FUS, FUS mutants, and RNA constructs

Plasmid preparation

Bacterial expression plasmids for wild-type FUS and all the ALS mutant variants were fused to a 6-HIS tag and an MBP tag at the N terminus. Plasmids were designed and order via gene synthesis and codon-optimized for expression in *E. coli* (pTHMT/FUS), by Genscript (Piscataway, NJ). All bacterial constructs encode a protease cleavage site between the 6xHIS-MBP tag and the FUS gene.

Protein Purification

FUS was purified using Ni-Affinity columns. 6xHis-MBP-FUS (wild-type and mutants) expression plasmids were transformed into BL21 (DE3) competent *E. coli* cells (NEB). Cells were grown at 37°C till OD600 reached 0.4, when protein expression was induced by 0.25mM IPTG. Proteins were expressed at 30°C for 2h. Harvested cell pellets were lysed by sonication (Lysis Buffer: 1MKCl, 1 M Urea, 50mM Tris-HCl, pH 7.4, 10mM imidazole, 1.5mM β-mercaptoethanol, 1% NP-40, 5% glycerol, and protease inhibitor tablet), followed by centrifugation at 20,000 g for 1 h at 4°C. The supernatant was passed through a HISTRAP HP column (GE), using an AKTA pure 25M FPLC system (GE). Proteins were eluted using a gradient of imidazole (Elution Buffer: 1M KCl, 1 M Urea, 50mM Tris-HCl, pH 7.4, 1.5mM β-mercaptoethanol, 5% glycerol, 500mM imidazole). FUS-containing fractions showing the correct size corresponding were pooled and stored in 30% Glycerol at 4°C.

RNA sample preparation

The following single strand modified RNA oligonucleotides were purchased from IDT:

(1) 18-mer: 5′-biotin-UGG CGA CGG CAG CGA GGC-3′-amino modified;
(2) U(10 to 70)-18-mer: 5′-amino modified-$(U)_{10\text{-}70}$GCC UCG CUG CCG UCG CCA-3′;
(3) U40: 5′-$(U)_{40}$-3′-amino modified.

Amino modified RNA strands were end-labeled with Cy5 or Cy3 via NHS-ester-amine chemistry.

For smFRET and EMSA, RNA substrate pdU50 was generated as follows: Partially complementary single RNA strands 18-mer and U50-18-mer (strands 1 and 2), labeled with Cy5 and Cy3, repectively, were annealed by mixing them at 1:1 molar ratio in appropriate buffer (10 mM Tris-HCl, pH 7.5, 100 mM NaCl), heating to 85°C for 2 min, followed by slow cooling (1°C per min) to room temperature. Annealing was verified by gel electrophoresis on 6% DNA retardation gel from Invitrogen.

For phase separation assay, a mixture of unlabeled U40 (strand 3) and Cy3-labeled U40 were used (100:1 ratio, respectively)

Characterization of WT FUS and FUS mutants

Slide Surface Preparation

For all the single molecule experiments passivated PEG slides were used. In brief, quartz slides and glass coverslips were thoroughly washed in Methanol and Acetone. Next they were sonicated in 1M KOH for 30min and flamed for 30 s. The slides and coverslips were coated with aminosilane for 20 minutes, then treated with a mixture of 98% mPEG (m-PEG-5000, Laysan Bio, Inc.) and 2% biotin PEG (biotin-PEG-5000, Laysan Bio, Inc) over night. The slides and coverslips were then washed a dried using nitrogen gas and stored in -20°C.

Single molecule FRET and PIFE measurements

All smFRET assays were performed at room temperature. Dual FRET pair (Cy5/Cy3)-labeled or Cy3 labeled PIFE RNA substrates were immobilized on PEG-passivated quartz slides via biotin-Neutravidin linkage. For protein-RNA interaction smFRET experiments, purified 6xHIS-MBP-FUS was applied on the slide, in imaging buffer containing an oxygen scavenger system to stabilize fluorophores (20 mM Tris-HCl, pH 7.5, 100 mM KCl, 0.5 w/v % glucose, 1 mg/mL glucose oxidase, 1.8 U/mL catalase, 5-10 mM trolox). Movies were recorded over different regions of the imaging surface, using a home-built prism-type TIRF-FRET microscope.

The flow experiments were done using a syringe pump. The pump was used to withdraw 50μL at a rate of 1mL/min with 10 s delay after the start of the recording.

EGFP photobleaching measurements

Partially duplex U50 RNA (pdU50) only labeled with Cy5 was immobilized on the surface of the PEG slide. EGFP fused WT FUS was introduced to the slides at varying concentrations (2.5-50nM) with buffere containing 20mM Tris and 100mM KCl. Movies were acquired from different regions of the slide while the sampled was excited by 488nm laser to bleach the EGFP molecules.

For subtracting the inherent dimerization of EGFP from the photobleaching step measurements, 5nM WT FUS::EGFP was added on the surface of slide primed with 10nM anti-GFP antibody for 15min then bleached using a 488nm laser. The photobleaching steps were counted and the dimer and multimer fraction was used as to subtract the background.

Electrophoretic Mobility Shift Assay (EMSA)

Ensemble RNA-protein interaction was assayed via EMSA. Briefly, 0.5-1 nM dual (Cy5/Cy3)-labeled RNA substrate (same as used in smFRET assay) and protein (6xHIS-MBP-FUS) at varying concentrations were mixed in appropriate buffer (50mM Tris-HCl, pH 7.5, 150mM KCl, 2mM $MgCl_2$, 100mM β-mercaptoethanol, 0.1mg/mL BSA), and incubated at room temperature for 30 min. Reaction mixtures were mixed with loading dye and species separated by electrophoresis on a 6% DNA retardation polyacrylamide gels (Invitrogen). Gels were imaged using fluorescence mode on a Typhoon scanner (GE Healthcare). Quantifications on the EMSA gels were performed using ImageQuantTL software.

Phase separation and C_{sat} measurements

Purified 6xHIS-MBP-FUS protein (that was stored in 1M KCl, 1 M Urea, 50 mM Tris-HCl, pH 7.4) was buffer exchanged with 20mM sodium phosphate pH 7.4 buffer, using centrifugal filters 30kDa molecular weight cutoff (Amicon, Millipore). 1 μM of buffer-exchanged protein was mixed with RNA 1μM unlabeled 40nt long polyU RNA (U40) and 10nM Cy3-labeled U40] in buffer (100 mM Tris-HCl, pH 7.5, 100 mM NaCl, 1 mM EDTA, 1 mM DTT). Phase separation and droplet formation was initiated by adding the appropriate amount of TEV protease to cleave the MBP tag. Droplets formed on the surface of an 8-well Nunc Lab-Tek chambered coverglass were imaged over time, using a Nikon Ti Eclipse microscope with a 100x oil immersive objective spanning an area of $\sim$133 $\times$ 133μm^2, at 555nm with a Cy3 emission filter and an EMCCD Andor camera.

For measuring the saturation concertation, droplets were formed at varying concentrations (0.3-2μM) using the same methods described above. In order to quantify droplet formation, we used the intensity-based cell counting macro from NIS-Element AR software provided by Nikon, extracting the number and size distribution of the droplets at each time point. Then, the data were plotted using Origin Pro 8.5.

Fluorescent Recovery After Photobleaching (FRAP) measurements

FRAP experiments were done using the same microscope with a 50mW bleaching laser at 405nm and a Brucker galvano mirror scanner. Multiple granules were bleached completely in the same field of view (ROI of 10-20 pixels in diameter) for 5ms per pixel using 50% laser intensity. Acquiring data for the recovery resumed immediately after bleaching using a 555nm excitation laser with a Cy3 emission filter at every 3 s for the first 2 minutes and every 10 s for the rest of the time points.

Fluorescent Anisotropy

Fluorescence anisotropy experiments were carried out on Thermo Scientific Nunc MicroWell 96-well microplates (Cat # 152038). Binding reactions were incubated on the plate for one hour. Following the incubation period, fluorescence polarization was measured using a TECAN Spark 10M plate reader with fluorescent excitation at 563 nm and emission at 615 nm (20 nm bandwith).

QUANTIFICATION AND STATISTICAL ANALYSIS

Single molecule FRET and PIFE

All the traces single molecule traces were visualized and analyzed using customized MATLAB codes.

FRET histograms and time traces for each experimental condition were generated from thousands of single molecules recorded over $\sim$20 movies.

To quantify dynamics of RNA-protein interaction, we measured the time between consecutive FRET events for each condition (dwell time) using a custom MATLAB code. Similar quantification was performed to measure the binding time in different PIFE constructs. Histogram of these data was fit with an exponential decay and the decay time was extracted.

The FRET heatmaps were generated by an in-house MATLAB script overlaying more than 100 traces synced by the start of each trace.

To quantify the different mutant smRET traces, we measured the fraction of time in which each molecule spends time in the dynamic state (non-static state). More than 150 traces were used in each case. The values (from 0 to 1) were then plotted using a violin plot MATLAB script.

EMSA gel quantification

Quantifications on the EMSA gels were performed using ImageQuantTL software. Intensities of each band was normalized based on the total intensity of each lane after background subtraction.

Phase separation and C saturation

In order to quantify droplet formation, we used the intensity-based cell counting macro from NIS-Element AR software provided by Nikon, extracting the number and size distribution of the droplets at each time point. Then, the data were plotted using Origin Pro 8.5.

For measuring the C saturation, the total area covered by the droplets were measured as a function of FUS concentration using NIS-Element AR software. The C_{sat} was defined as the intersection between the fit of the linearly growing region of the graph and the x axis. In other words, the concentration of the protein in which the droplets start to form.

FRAP analysis

The FRAP data were analyzed using a custom MATLAB 2015b code. The average fluorescent intensity of each ROI was recorded over time and corrected for the general fluorescent bleaching using the equation below:

$$I_{corr}(t) = \frac{I(t) - B}{I_{ref}(t) - B}$$

where, B is the background, I_ref (t) is the intensity of an unbleached droplet at any given time, and I(t) is the intensity of the bleached spot. The corrected intensity is then normalized as follows:

$$I_{norm}(t) = \frac{I_{corr}(t) - I_{corr}(bleached)}{I_{corr}(prebleached) - I_{corr}(bleached)}$$

where, $I_{corr}(bleached)$ and $I_{corr}(prebleached)$ are the intensity of the bleached droplet immediately after and before bleaching, respectively.

Fluorescent Anisotropy

Anisotropy was calculated using the following equation:

$$r = 1000 \times \frac{I_p - I_e}{I_p + 2\,I_e}$$

Where Ip is the parallel fluorescence emission and Ie is the perpendicular fluorescence emission. For Kapβ2 competitive binding assays, the wild-type FUS and Cy3-U40 RNA concentrations were held constant at 100 nM and 10 nM, respectively, while Kapβ2 concentration was varied from 1 μM to ~15 pM via successive 1:2 dilutions. All reactions were carried out in Binding Buffer (see Electrophoretic Mobility Shift Assay (EMSA) section).

DATA AND CODE AVAILABILITY

Single Molecule FRET data acquisition and analysis package can all be obtained freely from the website (https://cplc.illinois.edu/software/).

IDL (http://www.exelisvis.co.uk/ProductsServices/IDL.aspx) and MATLAB (https://www.mathworks.com/) software with academic or individual licenses can be obtained from their respective software companies.

Violin plot MATLAB code was available online through MATLAB file exchange (https://www.mathworks.com/matlabcentral/fileexchange/45134-violin-plot)

OriginLab (https://www.originlab.com/) software with academic or individual licenses can be obtained from the software company.